ACS APPLIED ENERGY MATERIALS
Cite This: ACS Appl. Energy Mater. XXXX, XXX, XXX−XXX
Letter
www.acsaem.org

Transparent Quasi-Interdigitated Electrodes for Semitransparent Perovskite Back-Contact Solar Cells

Giovanni DeLuca,[†,‡,§,○] Askhat N. Jumabekov,[‡,○,◆] Yinghong Hu,[‡,∥] Alexandr N. Simonov,[⊥,#] Jianfeng Lu,[§] Boer Tan,[§] Gede W. P. Adhyaksa,[¶] Erik C. Garnett,[¶] Elsa Reichmanis,[*,†,&] Anthony S. R. Chesman,[*,‡,▽] and Udo Bach[*,§,▽,^]

[†]School of Chemistry and Biochemistry, Georgia Institute of Technology, Atlanta, Georgia 30332, United States
[‡]CSIRO Manufacturing, Clayton, Victoria 3168, Australia
[§]Department of Chemical Engineering, Monash University, Clayton, Victoria 3800, Australia
[∥]Department of Chemistry and Center for NanoScience (CeNS), LMU Munich, 80539 Munich, Germany
[⊥]School of Chemistry, Monash University, Clayton, Victoria 3800, Australia
[#]ARC Centre of Excellence for Electromaterials Science, Monash University, Clayton, Victoria 3800, Australia
[¶]Center for Nanophotonics, AMOLF, 1098 XG Amsterdam, The Netherlands
[&]School of Chemical and Biomolecular Engineering, Georgia Institute of Technology, Atlanta, Georgia 30332, United States
[▽]Melbourne Centre for Nanofabrication, Clayton, Victoria 3168, Australia
[^]ARC Centre of Excellence for Exciton Science, Monash University, Clayton, Victoria 3800, Australia

Supporting Information

ABSTRACT: Transparent quasi-interdigitated electrodes (t-QIDEs) were produced by replacing the opaque components of existing QIDEs with indium tin oxide (ITO). We demonstrate their application in the first semitransparent back-contact perovskite solar cell. A device with a V_{OC} of 0.88 V and a J_{SC} of 5.6 mA cm^{-2} produced a modest 1.7% efficiency. The use of ITO allows for illumination of the device from front and rear sides, resembling a bifacial solar cell, both of which yield comparable efficiencies. Coupled optoelectronic simulations reveal this architecture may achieve power conversion efficiencies of up to 11.5% and 13.3% when illuminated from the front and rear side, respectively, using a realistic quality of perovskite material.

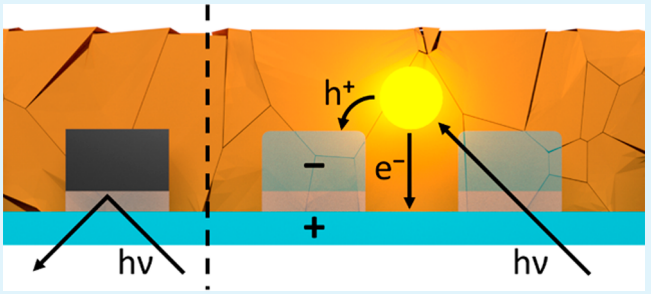

KEYWORDS: *back-contact solar cell, perovskite solar cell, coupled optical-electrical modeling, transparent conducting oxides, transparent quasi-interdigitated electrodes*

While back-contact electrodes (BCEs) are incorporated into the highest efficiency silicon solar cells,[1] they are yet to be adopted by researchers fabricating organometal halide perovskite analogues. The fabrication of back-contact perovskite solar cells (BC-PSCs) will eliminate parasitic absorption by the top contact and leave the perovskite surface exposed, allowing for improvements through light-trapping, the application of an antireflective coating, new post-annealing techniques, surface passivation, and photoluminescence out-coupling.[2,3] Furthermore, the architecture offers several functional advantages during fabrication, including the elimination of shorting due to pinholes, and avoiding damage to the perovskite layer during the deposition of subsequent layers.[4] However, the electrode spacing in the BCEs currently used in Si solar cells is too large for perovskites, which have shorter carrier diffusion lengths. Also, the processes used to fabricate commercial BCEs are not compatible with perovskite thin films,[5] thus prohibiting the direct transfer of existing technology to this new class of photoabsorber material.

The realization of operational BC-PSCs therefore necessitated the development of a new device architecture, namely, quasi-interdigitated electrodes (QIDEs) (Figure 1a). This back-contact architecture places a finger-shaped cathode onto a continuous thin-film anode, with an insulating layer separating the electrodes. This avoids formation of the short-circuit pathways that occur in conventional coplanar interdigitated electrodes when a defect in one electrode finger causes contact with an adjacent electrode, a problem that increases in frequency as the electrode features are miniaturized to the

Received: July 11, 2018
Accepted: August 20, 2018
Published: August 20, 2018

DOI: 10.1021/acsaem.8b01140
ACS Appl. Energy Mater. XXXX, XXX, XXX−XXX

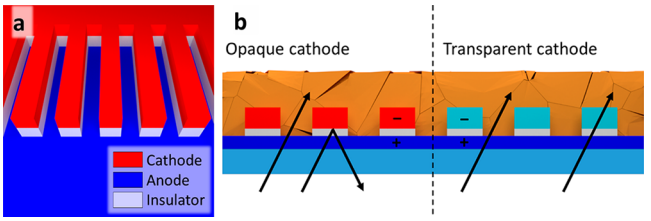

Figure 1. (a) Structure of a QIDE. (b) Light transmission, absorption, and reflection in QIDEs with Al/NiCo electrodes (left) or transparent electrodes (right).

dimensions required for the charge carrier diffusion lengths of perovskites.[4]

Although QIDEs present a robust architecture for BC-PSCs, a key design element limits their potential application. The top contacts are currently composed of opaque Al|NiCo fingers, which are strong absorbers/reflectors of incident light (Figure 1b), preventing their use in semitransparent PSCs or as the top electrode in tandem perovskite-silicon solar cells. Therefore, for QIDEs to reach their full potential, the top electrode must be replaced with a transparent conductor. To this end, we introduce herein the first transparent quasi-interdigitated electrodes (t-QIDEs) based on indium tin oxide (ITO), which has a high carrier concentration, low sheet resistance, and most importantly, higher optical transmittance (>85% in visible wavelengths) than Al|NiCo.[6] Furthermore, we demonstrate the first operational semitransparent back-contact perovskite solar cell. Optoelectronic theoretical simulations[2] also show the realistically achievable power conversion efficiencies (PCEs) and average visible transmissions (AVT) with varying perovskite film thicknesses.

Creating t-QIDEs first required optimization of the deposition of ITO that replaced the opaque components in the original architecture. This was achieved by varying the following deposition parameters: substrate temperature, ITO target power, argon and oxygen flow rates, and post-deposition annealing conditions. The optimized process yielded ~200 nm ITO thin films with an optical transmittance of ca. 88% at 592 nm (Figure S1), and sheet resistances ranging from 25 to 35 Ω $\square^{-1}$. Photoelectron spectroscopy in air (PESA) measurements confirmed the ITO had a work function (4.78 ± 0.08 eV) comparable to literature values (Figure S2 and Table S1).[7]

Post-deposition annealing for 3 min at 300 °C was required to enhance transmittance in the solar spectrum region (Figure S1). This accompanied the transformation of fully amorphous ITO to a highly crystalline phase, as evidenced by X-ray diffraction (XRD) measurements (Figure S3). In addition, postdeposition annealing resulted in a 20-fold decrease in sheet resistance. While heating the substrate during ITO deposition is preferable to postdeposition annealing,[8,9] the high temperatures required for the former process are not compatible with the photoresist used during t-QIDEs fabrication; therefore, the sample required the postannealing process.

Once optimized, a deposition parameters were applied to the fabrication of ITO fingers for t-QIDEs. The initial electrode fabrication steps followed previously reported work,[4] where a photoresist served as the negative of the electrode pattern applied to a FTO|TiO_2 stack on glass, followed by the deposition of an Al_2O_3 insulating layer to separate the anode and cathode. A continuous thin film of ITO was then deposited, and subsequent lift-off of the photoresist mask afforded ITO electrode fingers. Images taken following lift-off revealed the mask was completely removed and the ITO fingers were undamaged (Figure S4). After the photoresist mask was removed, the electrodes were annealed, transforming the electrodes from light-brown to colorless (Figure 2a).

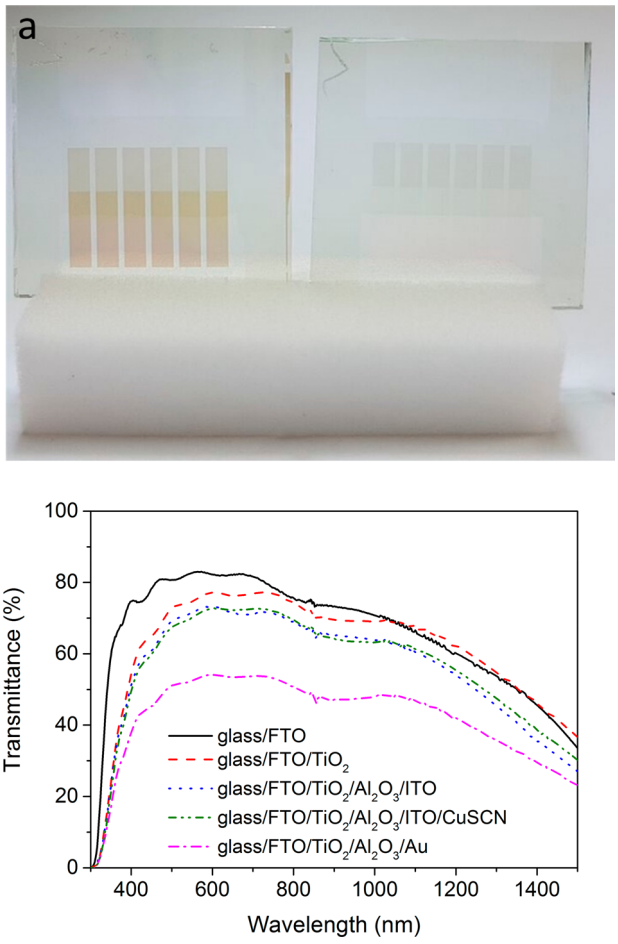

Figure 2. (a) Photograph of t-QIDEs before (left) and after annealing at 300 °C (right). (b) UV−vis−NIR transmission spectra of the t-QIDEs at various stages of fabrication and for a QIDE with a gold top electrode.

Finally, to ensure the electrodes have the necessary band energy alignment with a perovskite photoabsorber, a suitable hole transport material, copper(I) thiocyanate, was electrodeposited onto the ITO fingers prior to perovskite deposition.

UV−vis−NIR spectroscopy measurements were performed on the electrode stack at each stage of the fabrication process to determine the contribution of each component to the incident light absorption of the t-QIDEs (Figure 2b, Table S2, and Table S3). The pristine FTO-coated glass exhibited the highest transmittance, while TiO_2 deposition resulted in a slight drop in transmittance in the blue and visible regions of the spectrum. After the Al_2O_3|ITO top electrode was deposited (quasi-interdigitated area), the overall transmittance decreased by approximately 15% and 10% relative to the FTO-coated glass substrate and FTO|TiO_2 anode, respectively. This results mainly from the formation of additional interfaces (TiO_2|Al_2O_3 and Al_2O_3|ITO), which enhance the reflectance of the electrode assembly. The addition of the hole transport layer caused insignificant changes to the average transmittance (Figure 2b). The t-QIDE architecture is an ordinary reciprocal

DOI: 10.1021/acsaem.8b01140
ACS Appl. Energy Mater. XXXX, XXX, XXX−XXX

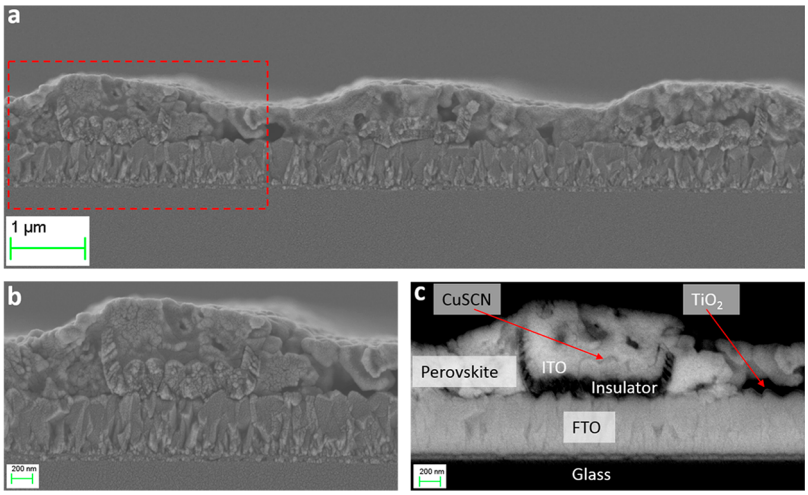

Figure 3. (a) Cross-sectional SEM image of the back-contact PSC based on the $Cs_{0.05}FA_{0.79}MA_{0.16}PbI_{2.49}Br_{0.51}$ photoabsorber and a t-QIDE, (b) high magnification cross-sectional SEM image of the device (area enclosed with red rectangle in Figure 3a), (c) backscattered SEM cross-sectional image of a finger of the device (area enclosed with red rectangle in Figure 3a).

system that gives identical transmission through both sides, with insignificant differences probably arising from scattering (Figure S5). To demonstrate the transparency of the ITO fingers, identical measurements were performed on a device where ITO was replaced with a ca. 60 nm thick layer of gold. This substitution resulted in a significant decrease in transmission to ca. 50%, confirming that the relatively high transmittance of the t-QIDEs is due to the transparent nature of ITO (Figure 2b).

While t-QIDEs could potentially be applied to a range of photoabsorber materials, CuSCN was applied to the ITO to provide a band energy alignment compatible with hybrid organic–inorganic perovskites (Figures S6 and S7). For this study we selected a multiple-cation mixed-halide perovskite with the nominal composition $Cs_{0.05}FA_{0.79}MA_{0.16}PbI_{2.49}Br_{0.51}$ as the photoabsorber, which has shown high photovoltaic efficiencies.[10] Figure 3a presents a cross-sectional scanning electron micrograph of a back-contact PSC based on a t-QIDE. The backscattered electron image of an individual finger reveals that a thin perovskite layer (~340 nm) uniformly covers the t-QIDE, which consists of a microstructured cathode (~1.5 μm wide ITO|CuSCN fingers spaced every ~2.5 μm) on a continuous anode (FTO|TiO_2 on glass), separated by ~100 nm of Al_2O_3 (Figure S8). The microfingers of the cathode were trough shaped rather than perfectly flat, due to the polymer mask fabrication process where the edges of the grooves formed by the mask are imperfectly defined. A backscattered electron cross-section image provides additional contrast to differentiate the functional device layers (Figure 3c).

The J–V characteristics of BC-PSCs with t-QIDEs were recorded with both front (perovskite) and rear (glass) side illumination. Figure 4a shows J–V curves under 1 sun AM1.5G illumination and in the dark, while relevant photovoltaic parameters are summarized in Table S4. With front side illumination, values of 5.5 mA cm^{-2}, 0.84 V, and 30% were recorded for short-circuit current density (J_{SC}), open-circuit voltage (V_{OC}), and fill factor (FF), respectively, yielding a PCE value of 1.4% for a reverse scan. For rear side illumination and reverse scan, a slightly higher PCE value of 1.7% was obtained, with J_{SC}, V_{OC}, and fill factor being 5.6 mA cm^{-2}, 0.88 V, and 34%, respectively. As expected, excluding CuSCN from t-

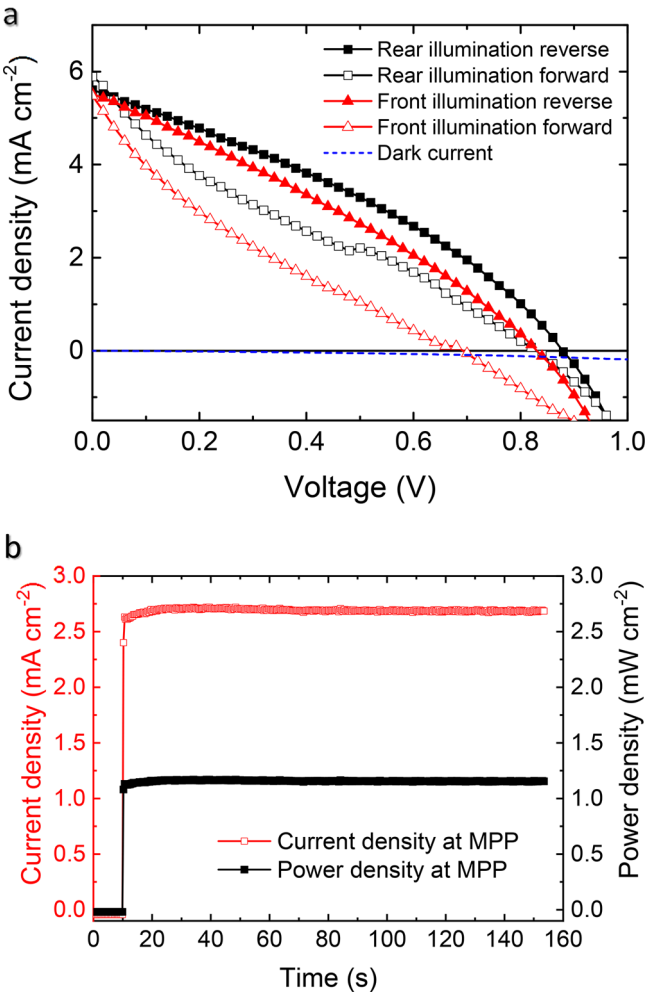

Figure 4. (a) J–V characteristics (scan rate 0.2 V s^{-1}) of a BC-PSC based on the $Cs_{0.05}FA_{0.79}MA_{0.16}PbI_{2.49}Br_{0.51}$ photoabsorber and a t-QIDE measured under 1 sun illumination from the front (perovskite) side and rear (glass) side and in the dark. (b) Evolution of photocurrent and power density of the same BC-PSC at maximum power point under 1 sun irradiation from the rear side.

DOI: 10.1021/acsaem.8b01140
ACS Appl. Energy Mater. XXXX, XXX, XXX–XXX

QIDEs resulted in lower device performance, demonstrating the advantages provided by having a hole-selective layer (Figure S9). The $J-V$ curves exhibit hysteresis, which is typically assigned to ion migration and interfacial charge recombination.[11] The maximum power point (MPP) for the best-performing device irradiated with 1 sun from the rear showed a stable output with a PCE value of ca. 1.2% maintained for at least 140 s (Figure 4b).

A potential application of t-QIDEs is in semitransparent perovskite solar cells. While the PCEs of the current devices are notably below the state-of-the-art for back-contact solar cells, future increases in efficiency are anticipated through increased perovskite grain sizes, a decreased sheet resistance of the transparent electrodes, and improved deposition procedures for the hole transport layer. To determine whether our device architecture could realistically reach the PCE and AVT of the previously reported semitransparent solar cells,[12,13] coupled optical and electrical simulations were performed using previously reported physical characteristics for key components (Table S5).[2]

The simulations used a realistic quality of perovskite material with a minority-carrier diffusion length of 500 nm. Figure 5a shows the simulated evolution of PCE as a function of perovskite layer thickness with a t-QIDE with optical and electrical properties as defined in this study. The simulations revealed an overall efficiency that is always higher when the cell is illuminated from the glass/electrode interface (rear illumination) vs the air/perovskite interface (front illumination), which supports the experimental observations. A fluctuation in the PCE originates from a combination of thin-film interferences and drift-diffusion carrier transport and becomes more pronounced with rear illumination due to a higher number of modes evolved passing through the multilayer structure.[14] When the device is illuminated from the front or rear side, the simulated maximum efficiency is ca. 12% (at 750 nm perovskite thickness) or ca. 13% (at 650 nm perovskite thickness), respectively. Rear illumination requires a ~50 nm thinner perovskite layer to reach a similar efficiency to front illumination, which also suggests more efficient charge collection.

Figure 5a also demonstrates the potential of BC-PSCs to act as semitransparent devices when thin layers of perovskite absorber are employed. The AVT is calculated between 400 and 800 nm for comparison with reported work.[12,13] For the thinnest perovskite layer needed for the PSC to be operational, viz. 250 nm, which is the thickness of the back-contact electrode, a potential AVT of 32% was calculated. Corresponding PCE values were predicted as 5.9 and 7.5% for the devices irradiated from the front and rear, respectively (Table S6). These values are comparable to previous reports for tandem organic photovoltaics.[15] At the maximum efficiencies, AVTs of 9.1% (front illumination, PCE = 12%) and 11% (rear illumination, PCE = 13%) were calculated, demonstrating potentially superior performance.[12,13] The back-contact architecture also permits the application of an antireflective coating, light trapping, surface passivation, and photoluminescence out-coupling enhancements, which are expected to improve both the PCE and AVT of an optimized device.[2]

To identify the contribution to charge collection efficiency across the spectrum, the external quantum efficiency (EQE) of a BC-PSC at the optimal conditions for front and rear illumination was simulated (Figure 5b). In the short wavelength range (up to 430 nm), front illumination is more

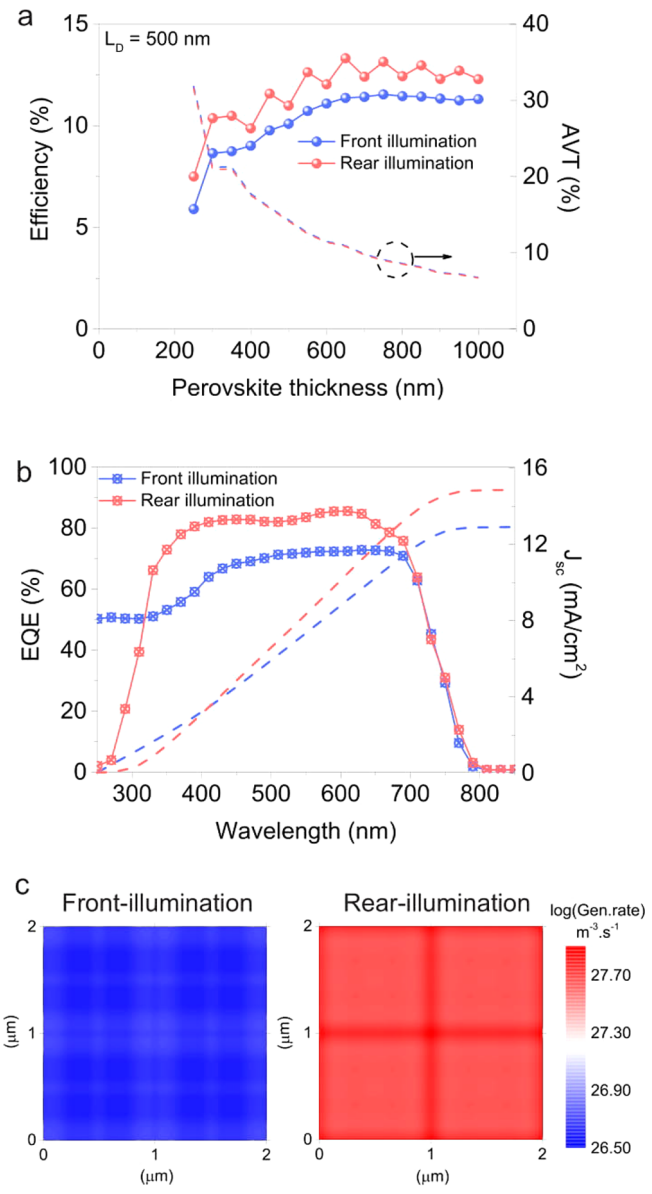

Figure 5. Simulated performance of a BC-PSC under front and rear illumination. (a) PCS and AVT as a function of perovskite thickness (the perovskite thickness cannot be below the thickness of the back-contact electrode, viz. 250 nm). (b) External quantum efficiency (EQE) at the optimum thickness of the perovskite layer (750 and 650 nm for front and rear illumination, respectively). (c) Charge generation rate of the perovskite layer between the two back-contact electrodes. The generation rate is averaged over the thickness of the perovskite and leveled to the total thickness of the electrodes. The apparent interference fringes are due to optical modes created by the multilayered structure evolved. Simulations were based on the AM1.5 spectrum and a 500 nm minority-carrier diffusion length for the perovskite.

efficient due to the absence of any parasitic absorption layer (ITO) in the first optical path of the incoming photons. In contrast, with rear illumination, the collection efficiency is higher within the higher wavelength range (430–780 nm), resulting in an increased accumulated J_{sc}. This is partly due to better index-matching between the glass|ITO|perovskite interfaces than the air|perovskite interface, effectively creating an antireflective coating that minimizes total reflectance. This leads to increased absorption in the perovskite, and a higher

DOI: 10.1021/acsaem.8b01140
ACS Appl. Energy Mater. XXXX, XXX, XXX−XXX

charge photogeneration rate near the back-contact electrode (Figure 5c). An order of magnitude difference for the rear and front illumination conditions (Figure 5c) explains the experimentally observed difference in J_{sc} (Figure 4a and Table S6).

Simulations undertaken herein suggest that further optimization of devices with t-QIDEs should be possible by minimizing parasitic losses. For example, this can be achieved by increasing the spacing gap size between the back-contact (for a fixed back-contact width), if possible with a better quality of perovskite material (e.g., with minority-carrier diffusion length $L_D > 10$ μm) (Figure S10a). Alternatively, increasing a filling fraction of the back-contact electrode is seen as a promising strategy for a realistic quality of perovskite ($L_D \approx 0.5$ μm). Unlike devices incorporating metal electrodes, the PCE is less sensitive to the width of the ITO back-contact finger (Figure S10b).[16]

In summary, the fabrication of a transparent back-contact electrode was achieved by replacing the opaque components of conventional QIDEs with ITO. These electrodes were used as substrates for the first semitransparent back-contact perovskite solar cells with a modest PCE of 1.2%. Importantly, this new class of devices offers straightforward strategies for optimization that could significantly increase the efficiency. Simulations showed that if these improvements can be achieved, BC-PSCs incorporating t-QIDEs will offer a pathway to efficient semitransparent photovoltaic devices.

■ ASSOCIATED CONTENT

Supporting Information

The Supporting Information is available free of charge on the ACS Publications website at DOI: 10.1021/acsaem.8b01140.

Experimental details including materials, transparent quasi-interdigitated electrode fabrication, deposition of CuSCN layer, PV device fabrication, characterization details, and details in simulation setup and device structures, UV−vis−NIR spectra and data, PESA measurement results, XRD patterns, visible light microscope image, table of transmission data, band diagram, high magnification backscattered electron cross sectional image, photovoltaic parameters, $J-V$ curves, physical parameters used in simulations, simulated PCE and AVT data, simulated PCE map (PDF)

■ AUTHOR INFORMATION

Corresponding Authors

*E-mail address: elsa.reichmanis@chbe.gatech.edu (E. Reichmanis),.

*E-mail address: anthony.chesman@csiro.au (A. S. R. Chesman).

*E-mail address: udo.bach@monash.edu (U. Bach).

ORCID

Giovanni DeLuca: 0000-0002-3456-1020

Askhat N. Jumabekov: 0000-0003-0051-9542

Yinghong Hu: 0000-0002-9630-1662

Alexandr N. Simonov: 0000-0003-3063-6539

Gede W. P. Adhyaksa: 0000-0003-3048-4627

Elsa Reichmanis: 0000-0002-8205-8016

Anthony S. R. Chesman: 0000-0002-1807-4468

Udo Bach: 0000-0003-2922-4959

Present Address

◆Department of Physics, School of Science and Technology, Nazarbayev University, Astana 010000, Kazakhstan.

Author Contributions

○Contributed equally to this work.

Notes

The authors declare no competing financial interest.

■ ACKNOWLEDGMENTS

We gratefully acknowledge the financial support from the National Science Foundation, NSF EAGER 1665279. G.D. is grateful for support from the NSF EAPSI program, OISE 1713327. E.R. thanks the Georgia Institute of Technology for support. E.R. additionally appreciates support from the Brook Byers Institute for Sustainable Systems at Georgia Tech. This work was performed in part at the Melbourne Centre for Nanofabrication (MCN) in the Victorian Node of the Australian National Fabrication Facility (ANFF). A.N.J. acknowledges an Office of the Chief Executive Postdoctoral Fellowship (CSIRO Manufacturing). Y.H. acknowledges funding from the DFG Excellence Cluster "Nanosystems Initiative Munich" (NIM), the Center for NanoScience (CeNS), and the Bavarian Collaborative Research Program "Solar Technologies Go Hybrid" (SolTech). The authors thank Mr. Mark Greaves and Dr Aaron Seeber from CSIRO Manufacturing for their help with SEM imaging and X-ray analysis, respectively. E.C.G. and G.W.P.A. acknowledge financial support from the European Research Council under the European Union's Seventh Framework Programme (FP/2007-2013)/ERC Grant Agreement 337328, "NanoEnabledPV". The authors also acknowledge the financial support from the Australian Renewable Energy Agency (ARENA), the Australian Centre for Advanced Photovoltaics (ACAP), and the Australian Research Council through the ARC Centre of Excellence in Exciton Science (CE170100026) and project DP160104575.

■ REFERENCES

(1) Yoshikawa, K.; Kawasaki, H.; Yoshida, W.; Irie, T.; Konishi, K.; Nakano, K.; Uto, T.; Adachi, D.; Kanematsu, M.; Uzu, H. Silicon Heterojunction Solar Cell with Interdigitated Back Contacts for a Photoconversion Efficiency over 26%. *Nat. Energy* **2017**, *2* (5), 17032.

(2) Adhyaksa, G. W.; Johlin, E.; Garnett, E. C. Nanoscale Back Contact Perovskite Solar Cell Design for Improved Tandem Efficiency. *Nano Lett.* **2017**, *17* (9), 5206−5212.

(3) Xiong, H.; DeLuca, G.; Rui, Y.; Li, Y.; Reichmanis, E.; Zhang, Q.; Wang, H. Solvent Vapor Annealing of Oriented PbI2 Films for Improved Crystallization of Perovskite Films in the Air. *Sol. Energy Mater. Sol. Cells* **2017**, *166*, 167−175.

(4) Jumabekov, A.; Della Gaspera, E.; Xu, Z.-Q.; Chesman, A.; Van Embden, J.; Bonke, S.; Bao, Q.; Vak, D.; Bach, U. Back-Contacted Hybrid Organic−Inorganic Perovskite Solar Cells. *J. Mater. Chem. C* **2016**, *4* (15), 3125−3130.

(5) Lu, G.; Wang, J.; Qian, Z.; Shen, W. Development of Back-Junction Back-Contact Silicon Solar Cells based on Industrial Processes. *Prog. Photovoltaics* **2017**, *25* (6), 441−451.

(6) Hartnagel, H.; Dawar, A.; Jain, A.; Jagadish, C. *Semiconducting Transparent Thin Films*; Institute of Physics Bristol, 1995.

(7) Helander, M.; Wang, Z.; Qiu, J.; Greiner, M.; Puzzo, D.; Liu, Z.; Lu, Z. Chlorinated Indium Tin Oxide Electrodes with High Work Function for Organic Device Compatibility. *Science* **2011**, *332* (6032), 944−947.

(8) Yan, L.; Schropp, R. Changes in the Structural and Electrical Properties of Vacuum Post-Annealed Tungsten-and Titanium-Doped

DOI: 10.1021/acsaem.8b01140
ACS Appl. Energy Mater. XXXX, XXX, XXX−XXX

Indium Oxide Films Deposited by Radio Frequency Magnetron Sputtering. *Thin Solid Films* **2012**, *520* (6), 2096−2101.
(9) Gupta, R.; Ghosh, K.; Mishra, S.; Kahol, P. High Mobility W-Doped In2O3 Thin Films: Effect of Growth Temperature and Oxygen Pressure on Structural, Electrical and Optical Properties. *Appl. Surf. Sci.* **2008**, *254* (6), 1661−1665.
(10) Saliba, M.; Matsui, T.; Seo, J.-Y.; Domanski, K.; Correa-Baena, J.-P.; Nazeeruddin, M. K.; Zakeeruddin, S. M.; Tress, W.; Abate, A.; Hagfeldt, A. Cesium-Containing Triple Cation Perovskite Solar Cells: Improved Stability, Reproducibility and High Efficiency. *Energy Environ. Sci.* **2016**, *9* (6), 1989−1997.
(11) Calado, P.; Telford, A. M.; Bryant, D.; Li, X.; Nelson, J.; O'Regan, B. C.; Barnes, P. R. Evidence for Ion Migration in Hybrid Perovskite Solar Cells with Minimal Hysteresis. *Nat. Commun.* **2016**, *7*, 13831.
(12) Roldan-Carmona, C.; Malinkiewicz, O.; Betancur, R.; Longo, G.; Momblona, C.; Jaramillo, F.; Camacho, L.; Bolink, H. J. High Efficiency Single-Junction Semitransparent Perovskite Solar Cells. *Energy Environ. Sci.* **2014**, *7* (9), 2968−2973.
(13) Della Gaspera, E.; Peng, Y.; Hou, Q.; Spiccia, L.; Bach, U.; Jasieniak, J. J.; Cheng, Y.-B. Ultra-Thin High Efficiency Semi-transparent Perovskite Solar Cells. *Nano Energy* **2015**, *13*, 249−257.
(14) Brongersma, M. L.; Cui, Y.; Fan, S. Light Management for Photovoltaics using High-Index Nanostructures. *Nat. Mater.* **2014**, *13* (5), 451.
(15) Chen, C.-C.; Dou, L.; Gao, J.; Chang, W.-H.; Li, G.; Yang, Y. High-Performance Semi-Transparent Polymer Solar Cells Possessing Tandem Structures. *Energy Environ. Sci.* **2013**, *6* (9), 2714−2720.
(16) Knight, M. W.; Van De Groep, J.; Bronsveld, P. C.; Sinke, W. C.; Polman, A. Soft Imprinted Ag Nanowire Hybrid Electrodes on Silicon Heterojunction Solar Cells. *Nano Energy* **2016**, *30*, 398−406.

■ NOTE ADDED AFTER ASAP PUBLICATION

This paper was published on the Web on August 23, 2018, before the author submitted their complete set of corrections. Additional text corrections were implemented throughout the paper, and the corrected version was reposted on August 27, 2018.

DOI: 10.1021/acsaem.8b01140
ACS Appl. Energy Mater. XXXX, XXX, XXX−XXX